Equilibrium and Stop-Flow Kinetic Studies of Fluorescently Labeled DNA Substrates with DNA Repair Proteins XPA and Replication Protein A

Lilia M. Iakoucheva,[‡,⊥] Randall K. Walker,[§] Ben van Houten,[§,#] and Eric J. Ackerman*[,‡]

Pacific Northwest National Laboratory (PNNL), Molecular Biosciences Department, P.O. Box 999, Richland, Washington 99352, and Sealy Center for Molecular Science, University of Texas Medical Branch, Galveston, Texas 77555-1071

Received May 21, 2001; Revised Manuscript Received October 24, 2001

ABSTRACT: Nucleotide excision repair (NER) is a crucial pathway in the maintenance of genome stability requiring at least two dozen proteins. XPA and RPA have essential roles in the damage recognition step of NER. To better understand the mechanism of their interactions with DNA, we utilized equilibrium and stop-flow kinetic approaches with fluorescently labeled oligonucleotides. Fluorescein is a bona fide NER lesion because a circular plasmid with a single defined fluorescein was repaired by efficient extracts from *Xenopus* oocyte nuclei. Single-stranded and double-stranded oligonucleotides 5′-labeled with fluorescein were used in the subsequent studies. Oligonucleotide fluorescence was quenched upon specific binding to full-length recombinant *Xenopus* XPA (xXPA) and/or human RPA. The binding was highly sensitive to the buffer conditions. Analysis of equilibrium binding data with ds DNA and xXPA revealed a single dissociation constant (K_d) of 24.4 nM. Stopped-flow kinetic experiments were described by a first-order on-rate constant k_{on} of 9.03×10^8 M^{-1} s^{-1} and k_{off} of 26.1 s^{-1}. From the ratio of off-rate to on-rate, a calculated K_d of 28.9 nM was obtained, revealing that the kinetic and equilibrium studies were consistent. The affinity of xXPA for ds undamaged DNA determined in our spectrofluorometry experiments was up to 3 orders of magnitude higher than previously reported values using different substrates, conditions, and assays [gel-shifts (EMSA), filter-binding, anisotropy, and surface plasmon resonance]. The same substrate DNA containing a 4-bp mismatch in the middle yielded a K_d five times higher (158 nM), indicating weaker binding by xXPA. The differences in K_d values for these two substrates were mainly attributable to the k_{on}, rather than k_{off} rates. Fluorescence intensity changes upon interaction of xXPA with ss 50-mer were too low to calculate an accurate K_d. Although recombinant human RPA binding to the ds 50-mer was very weak ($K_d > 1$ mM), stop-flow and equilibrium measurements to ss oligonucleotide yielded K_d values of 96 and 20.3 nM, respectively, which correlated with previously reported values using gel mobility shift assays and a similarly sized poly-dT. Equilibrium and stop-flow measurements to the cognate and mismatched ds oligonucleotides using both xXPA and hRPA yielded a 2- to 3-fold increase in the K_d.

DNA damage recognition in nucleotide excision repair (NER)[1] is poorly understood. Even the identity of the recognition proteins is controversial, with XPA, XPC-hHR23B, RPA, XPE, and TFIIH factors all exhibiting some preference for damaged DNA, reviewed in ref *1*. Furthermore, recognition can be affected by nucleosomes and it may differ for transcription-coupled repair vs global genome repair. Attempts by many investigators (*2*−*6*) to demonstrate strong specificity of the damage recognition protein XPA [or its *S. cerevisiae* homologue Rad14 (*7*)] for various NER substrates have revealed no more than a 3−4-fold XPA's preference for damaged vs. undamaged DNA. Sancar and co-workers (*8*) noted that XPA, RPA, or the combination of XPA and RPA have all been reported as the damage recognition factors, but that interestingly, none of these is capable of discriminating between cyclobutane thymine dimer-containing DNA and undamaged DNA on nonnucleosomal substrates using conventional electrophoretic mobility shift assays [EMSA]. Although both XPA and RPA can bind damaged DNA independently, RPA increases XPA's affinity for both undamaged and damaged DNA when added after XPA's interaction with DNA (*9*, *10*). RPA also directly interacts with XPA in the absence of DNA (*11*). XPC-HR23B has been proposed as the damage recognition factor (*12*), but some lesions can be excised without the need for this complex (*8*, *13*). XPC is not an obligatory factor for nontranscribed DNA; thus XPC is unlikely to be an essential damage-recognition protein (*1*). For at least the UV-induced pyrimidine (6−4) pyrimidone photoproduct in the absence of transcription, the most likely initial recognition occurs by XPA and RPA (*14*), not XPC-hHR23B. XPA is involved in interactions with RPA, ERCC1, and TFIIH, and of all known NER proteins, XPA is the only protein whose gene disruption completely obliterates NER (*1*).

* Corresponding author: eric.ackerman@pnl.gov; phone: 509 373 3595; fax: 509 376 2149.

‡ Pacific Northwest National Laboratory.

§ University of Texas Medical Branch.

⊥ Current address: School of Molecular Biosciences, Washington State University, Pullman, WA 99164-4660.

Current address: Program Analysis Branch and Laboratory of Molecular Genetics NIEHS, NIH, Research Triangle Park, NC 27709.

[1] Abbreviations: (6−4) lesion, pyrimidine (6−4) pyrimidone photoproduct; EMSA, electrophoretic mobility shift assay; NER, nucleotide excision repair; RPA, replication protein A; xXPA, *Xenopus* xeroderma pigmentosum group A protein.

10.1021/bi011041q CCC: $22.00
Published on Web 12/06/2001

Published K_d values for XPA binding different DNA substrates have varied from 10^{-5} M using gel shift mobility assays (*3*) to 10^{-8} M using filter binding (*15*), surface plasmon resonance (*16*), and fluorescence anisotropy (*17*). Only a 3-fold difference was observed between DNA containing lesions and undamaged DNA, with very weak binding to ss DNA (e.g., ref *18*). However, there is a recent report of 1.2×10^7 M^{-1} K_a for XPA binding an undamaged 49-mer, and 3.3×10^7 M^{-1} K_a for the same oligonucleotide containing a (6−4) lesion (*19*). Even NMR structures of human XPA's minimal DNA binding domain (MBD) with DNA (*15*, *20*, *21*) failed to elucidate the molecular basis for damage recognition. At the high protein−DNA concentrations required for NMR, one structure revealed contacts between the MBD and a short ss 9-mer (*21*).

We recently showed that about two-thirds of active, full-length XPA is very flexible, perhaps even structurally disordered (*22*, *23*). This finding is consistent with the hypothesis that unstructured domains can facilitate specific binding interactions between different molecules (*24*), i.e., a wide variety of DNA lesions or other repair proteins. Indeed, a disordered domain of XPA was recently shown to form an α-helix upon interaction with RPA (*25*).

A true understanding of the forces involved in complex formation requires thorough binding studies under varying conditions of temperature and salt concentration, and this type of investigation is problematic with gel-shift assays. Gel-shift binding studies can yield spurious results because this method is not an equilibrium assay, and complexes frequently dissociate during electrophoresis (*26*). Furthermore, gel-shift methods require low salt concentrations, and because protein−DNA interactions are highly salt dependent (*27*), the resulting data may not reflect cellular conditions.

The primary advantage of fluorescence assays is that they are performed in solution without requiring separation and quantitation of bound and free species. Furthermore, true equilibrium of complex formation can be obtained over a wide range of solution conditions and substrate concentrations since the sensitivity and dynamic range of fluorescence extends from millimolar to picomolar. Fluorescent measurements can also be applied to kinetic analysis at the millisecond time scale because reactions can be monitored continuously in real time over a broad range of reactant concentrations. Finally, reaction intermediates, stoichiometries, and many kinetic parameters in complex systems also can be discerned by fluorescence methods.

The present study utilizes kinetic and equilibrium approaches to investigate the steps involved in XPA ± RPA binding to DNA containing a single 5′-fluorescein. Interactions of XPA with DNA have not been examined previously by equilibrium and stop-flow methods, and previous studies used internal RPA fluorescence to investigate its binding to unlabeled ssDNA (*28*). After our work was completed, a fluorescence anisotropy study of XPA and RPA binding to a 3′-fluorescein oligonucleotides was published (*17*).

MATERIALS AND METHODS

Protein Expression and Purification. Plasmid pXPACXE1 containing the full-length *Xenopus laevis* XPA cDNA was a generous gift from Kenji Kohno, Nara Institute of Science and Technology, Nara, Japan. Recombinant xXPA was produced using pET-11a vector (Novagen, Madison, WI). Purified plasmid pET-11a-XPA was used to transform *Escherichia coli* BL21(DE3)pLysS host strain (Novagen). Cells were grown in a New Brunswick Scientific fermenter (3 L vessel, 2.5 L working volume) in the complex medium containing (g/L): tryptone, 15; yeast extract, 20; glycerol, 10. After heat sterilization of the sample and cooling to room temperature, the following ingredients were added (g/L): 15× phosphate buffer (KH_2PO_4, 34.6; K_2HPO_4, 188.2, heat-sterilized separately), a trace metals solution, 1 mL/L; iron-containing solution, 1 mL/L; $CaCl_2 \cdot 2H_2O$, 0.073; $MgSO_4 \cdot 7H_2O$, 0.25; thiamine, 0.001; ampicillin (freshly prepared), 0.1. The trace metals solution contained the following salts (g/L): $CoCl_2 \cdot 6H2O$, 2.4; $CuSO_4 \cdot 5H_2O$, 2.5; $NH_4Mo_7O_{24} \cdot 4H_2O$, 12.4; H_3BO_3, 0.62; $MnCl_2 \cdot 4H2O$, 2.0; $ZnCl_2$, 1.4 and 100 mL HCl/L. The trace metals solution was sterilized separately. The iron-containing solution was prepared by dissolving 27 g of $FeCl_3 \cdot 6H_2O$ in 100 mL of HCl and adjusting the volume with deionized water to a liter. Glucose solution (40% w/v, filter-sterilized) was added prior to inoculation to provide an initial glucose concentration of 10 g/L. Glucose was supplied constantly during fed-batch fermentation to maintain its final concentration in the growth media at 5 g/L.

Bacterial storage cultures used for inoculation of the fermenter were prepared as described (*29*). A total of 1−2 μL of storage culture was transferred on the agar plate containing 100 μg/mL ampicillin and 34 μg/mL chloramphenicol and grown at 37 °C. The single colony was transferred to a 4-L flask containing 500 mL complex media with appropriate antibiotics and grown at 37 °C until the OD_{600} reaches 1.0 and used to inoculate the fermenter. The pH during the fermentation was maintained at 7.0 by the controlled addition of 5 M NH_4OH solution; the dissolved oxygen level was maintained at 40% by agitation/DO_2/O_2 cascade that enriches the fermenter media with O_2 when the agitation speed reaches maximum (800 rpm); antifoam was added to suppress foaming. The fermenter culture was grown at 37 °C until the $OD_{600} \sim 10$. Before induction, the temperature was dropped to 30 °C, and the culture was induced by IPTG (1 mM final concentration). In 1.5 h after induction, rifampicin was added to 50 μg/mL and the culture growth was allowed to continue for 3 h at 30 °C. Cells were harvested by centrifugation and frozen at −80 °C. Total yield from 2.5 L of fermentation was 290 g of cells (wet weight).

All purification procedures were carried out at 4 °C unless indicated otherwise. Frozen cell paste was thawed on ice, resuspended in lysis buffer (50 mM Tris·HCl, pH 7.5; 100 mM KCl; 0.5 mM PMSF; 10 mM DTT; 1 mM EDTA; 10% glycerol; 0.01% NP-40; 1× antiprotease cocktail (13.3 μg/mL aprotinin, 6.6 μg/mL leupeptin, 6.6 μg/mL pepstatin), sonicated for 2 min and disrupted by two passages through a French press. The lysate was clarified by centrifugation at 100000*g* for 1 h. The supernatant was diluted with an equal volume of buffer A (20 mM Tris·HCl, pH 7.5; 100 mM NaCl; 10 mM DTT; 0.5 mM PMSF; 10% glycerol) and loaded onto POROS HQ50 anion exchange column equilibrated in buffer A. After loading, the column was washed with 12 column volumes of the same buffer, and a 10 column volume linear gradient of 100 mM to 1 M NaCl was used to elute xXPA. Fractions containing xXPA were identified by

10% denaturing polyacrylamide gel electrophoresis (SDS−PAGE), pooled, diluted 2.5-fold with buffer B (25 mM HEPES−KOH, pH 7.5; 100 mM KCl; 10 mM DTT; 10% glycerol) and loaded on the POROS HS20 cation exchange column. The column was washed with three column volumes of buffer B and developed with seven column volumes of linear gradient from 100 to 500 mM KCl, followed by two column volumes of 1 M KCl. The third hydrophobic interaction column PolyPROPYL A (PolyLC, Columbia, MD) was equilibrated with buffer C containing 0.9 M $AmSO_4$; 0.1 M sodium phosphate, pH 7.0; 10 mM DTT; 10% glycerol at room temperature; pooled fractions after POROS HS20 column were diluted twice with 2× buffer C and loaded on the third column. Column was washed with two column volumes of buffer C and pure xXPA was eluted by applying 13 column volumes of linear gradient from 0.9 to 0 M $AmSO_4$. The purified protein was dialyzed against storage buffer containing 50 mM Tris·HCl, pH 7.5; 200 mM KCl; 10 mM DTT; 20% glycerol, concentrated to 25−50 mg/mL (0.8−1.5 mM) using centrifugal ultrafiltration (Ultrafree, Millipore), quickly frozen in liquid nitrogen and stored at −80 °C until use.

DNA sequencing of the expression clone confirmed the expected sequence, as did N-terminal amino acid sequencing (done at University of Southern California, Comprehensive Cancer Center, Los Angeles, CA). The molecular weight of the full-length xXPA determined by ESI−FTICR mass spectrometry (30 922.02 Da) was consistent with the one predicted from the sequence (30 922.45 Da) assuming no posttranslational modifications (*22*).

The RPA expression clone was a gift from Prof. Marc Wold (University of Iowa), and RPA was purified as described (*30*).

Repair Reactions using Xenopus Nuclear Extracts. Xenopus systems have the highest known repair signal ever described for either cells or extracts [100% repair at high fidelity with no background synthesis on undamaged control substrate] (*31*). Complete repair reactions in oocyte nuclear extracts can be made dependent upon exogenous proteins (*31*). Repair of UV-irradiated plasmid is inhibited by antibodies to XPA in *Xenopus* nuclear extracts and is restored by adding purified recombinant full-length *Xenopus* XPA (*32*), thereby confirming activity of recombinant XPA.

Construction of DNA Substrates. The target oligonucleotides used in this study were (1) double-stranded 50-mer 5′-labeled with fluorescein [ds50] connected via an amide linkage to 6-carbon spacer attached to the phosphodiester; (2) single-stranded 5′-labeled 50-mer of the same upper-strand sequence [ss50]; (3) double-stranded 50-mer with 4 bp mismatch bubble in the middle—the upper strand was the same as in oligonucleotide (1) and in the bottom strand bold underlined bases were exchanged for TTTT [ds50−4M]; (4) covalently closed circular plasmid (7254 bp) with a single defined fluorescein connected via a thiourea to a 3-carbon spacer attached to the phosphodiester backbone. Fluorescein was attached during oligonucleotides synthesis and products were HPLC-purified (Oligos Etc., Wilsonville, OR). Duplex oligonucleotides were formed by annealing 50 μM of each DNA strand in 100 μL of 10 mM Tris-HCl, pH 8.0, 10 mM NaCl, 1 mM EDTA. The DNA strands were upper: 5′**F**TCTTCTCTTGATATCCTTCTTCTGGTCTTC-TCTTCAAGCTTCTCTCTCTT-3′; lower: 3′AGAAGAGAAC-TATAGGAAGAAG**ACCA**GAAGAGAAGTTCGAAGA-GAGAGAA-5′

The reaction was heated to 94 °C for 10 min and allowed to cool at room-temperature overnight. Duplexes were gel-purified from single-stranded oligonucleotides by electrophoresis on an 8% nondenaturing polyacrylamide gel. The duplex band was located on the gel with minimal necessary illumination with a hand-held UV lamp. The bands were excised, sliced, and soaked overnight at room temperature in 0.5 M NH_4OAc, 10 mM $MgCl_2$, 1 mM EDTA. The recovered supernatant was precipitated with 2 volumes of 95% ethanol containing 0.3 M NaOAc and 10 mM $MgCl_2$, incubated at −20 °C overnight, and DNA was recovered by centrifugation. The pellet was resuspended in 10 mM Tris HCl, pH 8.0, and stored at −20 °C until use. The DNA concentration was determined from absorbance at 260 nm using 1 OD equal to 50 μg/mL (absorbance of the fluorescein moiety at this wavelength is negligible). Necessary precautions were taken to minimize fluorescein photobleaching. Oligonucleotide sequences were designed primarily considering the availability of convenient restriction sites, an abundance of adjacent pyrimidines, and the presence of a single GG to facilitate formation of a cisplatin adduct for the future experiments.

Substrate (4) was prepared according to the following procedure.

Preparation of Plasmid Containing a Single Defined Fluorescein. The 56-mer ds oligonucleotides, 5′-**AATTC**G-CAGATCTGGCCTGATTGCGGTAGCGATGGAGCCGT-AACAGTACGTAGTCA-3′ and 5′-**AGCTT**GACTACGTA-CTGTTACGGCTCCATCGCTACCGCAATCAGGCC-AGATCTGCG-3′, were annealed and cloned into M13mp18 using *Eco* RI and *Hind* III sites (underlined) resulting in plasmid M13-LYM. Single-stranded form of the recombinant phage was purified as previously described (*33*) and annealed to the oligonucleotide containing fluorescein at the indicated (F) position, 5′-AGCTTGACTACGTACTGTTACGGCTC-CATC**F**CTACCGCAATCAGGCCAGATCTGCG-3′, which served as a primer for complementary strand synthesis with T7 DNA polymerase (New England BioLabs). Conditions were adopted from the Muta-Gene Phagemid in vitro mutagenesis kit (Bio-Rad, Hercules, CA). The 10× annealing buffer was 200 mM Tris-HCl, pH 7.4, 20 mM $MgCl_2$, 500 mM NaCl; 10× synthesis buffer: 5 mM each dNTP, 10 mM ATP, 100 mM Tris-HCl, pH 7.4, 50 mM $MgCl_2$, 20 mM DTT. For synthesis, BSA to final concentration 0.05 μg/μL was added. The experimentally determined optimum ratio of primer to template (ssDNA) was 40:1 with 500 ng of template (1 OD_{260} = 36 μg/mL for ss DNA) per 10 μL total reaction volume. Each annealing reaction contained 0.2 pmol of ss template, 6−9 pmol of primer, 1 μL of 10× annealing buffer; the reaction was scaled successfully to 50 mL final volume. Annealing was performed in a 70 °C water bath and cooled at a rate of approximately 1 °C/min to 30 °C over 40 min. The reaction was placed on ice, and the following solutions were added sequentially: 10× synthesis buffer, BSA to a final concentration of 0.05 μg/μL, 0.05 units/μL of T7 DNA polymerase, and 2 units/μL of T4 DNA ligase. The reaction was incubated 5 min at 25 °C, and then 2 h at 37 °C, followed by addition of identical quantities of fresh enzymes and incubation at 37 °C for another 5−6 h. Separation of form I from form II DNA was performed by

ultracentrifugation. To avoid nicking of the plasmid and photobleaching of the fluorescein, exposure to UV light was minimized for visualizing DNA bands and in all subsequent steps. EtBr was removed with Dowex AG50W-X8 resin (Bio-Rad) according to manufacturer's instructions. The final plasmid with a single defined fluorescein was ethanol precipitated, lyophilized, and stored at 4 °C in the dark until use. Generally 90% of ss DNA was converted to 80% of form I and 20% of form II, and up to 5 mg of fluorescein-labeled plasmid can be produced in the single 50 mL conversion reaction.

Electrophoretic Mobility Shift Assays [EMSA]. Indicated oligonucleotides (Genosys Biotechnologies, Woodlands, TX) were annealed with complementary strands and purified as described above:

5′-CTTCTTCTGGTCTTCTCTTC-3′ — 20-mer
5′-TTCTTCTGGTCTTCTCTT-3′ — 18-mer
5′-TCTTCTGGTCTTCTCT-3′ — 16-mer
5′-CTTCTGGTCTTCTC — 14-mer
5′-TTCTGGTCTTCT — 12-mer

Binding of 5 pM oligonucleotide and 25 pM xXPA (1:5 molar ratio) was in 25 mM HEPES−KOH, pH 7.5, 50 mM KCl, 5 mM $MgCl_2$, 1 mM DTT; 20 μL reaction was incubated at 30 °C for 30 min and then loaded on 8% native PAGE supplemented with 0.5 mM $MgCl_2$. Electrophoresis was in 0.5× TAE at 4 °C at 10 V/cm for 2 h, and gels were stained with SYBR Green I (Molecular Probes, Eugene, OR).

Fluorescence Measurements. Steady-state fluorescence measurements were done using a SPEX Fluorolog II spectrofluorometer. Stopped-flow measurements were performed either on an AVIV ATF105 spectrofluorometer with stopped flow option (Aviv Instruments Inc., Lakewood, NJ) or on a MOS-250 spectrofluorometer equipped with SFM-4/Q stopped-flow option (Molecular Kinetics Inc., Pullman, WA).

Emission Spectra. The emission spectra were recorded by scanning between 500 and 600 nm with the excitation wavelength set at 495 nm. The excitation spectra were recorded by scanning between 450 and 520 nm with the emission wavelength set at 520 nm. Slit-widths for oligonucleotides were usually 1−2 nm.

Equilibrium Studies. The fluorescence measurements were performed in one of the following buffers: 50 mM Tris-acetate, pH 7.5, 100 mM potassium acetate, 10% glycerol, 1 mM EDTA, 5 mM DTT [buffer D, ionic strength 0.15 M], or 25 mM HEPES−KOH, pH 7.5, 200 mM KCl, 5 mM $MgCl_2$, 5 mM DTT [buffer E, ionic strength 0.225 M], or 25 mM potassium phosphate, pH 7.0, 1 mM $MgCl_2$, 0.5 mM DTT, 150 mM KCl, 10% glycerol [buffer F, ionic strength ∼0.2 M]. All binding measurements were temperature controlled at 25 °C in a 160 μL quartz cuvette or 3-mL polymethacrylate disposable cuvettes with magnetic stirring. The titrations were performed by adding 1 μL of increasing concentrations of protein or protein complexes to 5−50 nM of oligonucleotide every two minutes. The change of the volume after the last titration point never exceeded 10% of the total binding reaction, and the data were recalculated accordingly using final volume correction. The measurements were taken after 2 min incubation when the fluorescence readings were stabilized. The change in fluorescence intensity was measured at 520 nm, following excitation at 495 nm for each titration point. The fluorescence intensity was measured every second for 10 consecutive seconds and then averaged. Heparin (Sigma) was added at the end of every titration experiment (*34*) to prove that the binding is reversible and the fluorescence signal returned to the initial value.

Error estimates were obtained from standard least-squares analysis. This was done by linear analysis about the optimized coefficients. The statistical uncertainty estimates were used to generate a covariance matrix for the raw data. Standard linear least-squares analysis was applied to construct the corresponding covariance matrix for the optimized coefficients. The quoted error limits were obtained from the diagonal components of this matrix (*35*).

Stopped-Flow Studies. Equal volumes of protein (at 10−100 nM) and DNA (at 10−25 nM) in the same buffers that were used for equilibrium measurements, from separate syringes were rapidly mixed in the stopped-flow instrument at 25 °C. Changes in fluorescence emission were measured at 520 nm after excitation at 495 nm (1−3 mm slits). Points were collected every 0.5 ms for 2 s. About 10−15 kinetic traces were routinely averaged for each experiment.

The error bars for k_{obs} values represent errors in the fit. The errors shown for the rate constants represent the mean of their deviation from computed maximum and minimum k_{obs} values. Errors for stop-flow K_d values were calculated by propagation of error analysis using the standard deviations in k_{on} and k_{off} [ignoring the cross-partial differential term (*36*)].

Data Analysis. The fluorescence intensity and stop-flow kinetic data were fit using SigmaPlot (Jandel Scientific) software. Equilibrium binding isotherms were fit to a simple bimolecular binding model by nonlinear regression, and stopped-flow kinetic traces were fit to single or sum of exponential to determine the rate constants.

Fluorescence intensity binding isotherms were fit to eq 1 by using nonlinear regression analysis:

$$F = F_0 + \frac{(F_{max} - F_0)}{2F_t}[(A_t + F_t + K_d) - \sqrt{(A_t + F_t + K_d)^2 - (4 \cdot A_t F_t)}] \quad (1)$$

where F is the observed fluorescence intensity, F_0 is the fluorescence intensity of free DNA, F_{max} is the fluorescence intensity of DNA bound to the protein, A_t is the total concentration of protein, F_t is the total concentration of DNA, and K_d is the dissociation equilibrium constant of the complex.

Anisotropy was calculated according to eq 2:

$$r = \frac{\frac{I_v}{I_h} - 1}{\frac{I_v}{I_h} + 2} \quad (2)$$

where I_v/I_h is the ratio of the measured intensities with vertical and horizontal excitation and corrected for instrumental bias of the detection system.

Binding isotherms were constructed under the simplifying assumption that the reactions were carried out under conditions where the DNA concentrations were adequately below the K_d such that total added protein was equivalent to free

protein. Because of quantum yield changes that occurred upon binding the anisotropy isotherms were constructed according to eq 3:

$$fb = \frac{r - r_f}{(r_b - r)R + r - r_f} \quad (3)$$

where *fb* is the fraction bound, *r* is the anisotropy at the given protein concentration, r_f is the anisotropy in the absence of protein, r_b is the anisotropy at saturating levels of protein, and *R* is the ratio of the quantum yields of the bound form and the free form, respectively.

Stopped-flow kinetic traces were fit to single-exponential eq 4:

$$F = y_0 + a \exp(-k_{obs}t) \quad (4)$$

or eq 5:

$$F = y_0 + a(1 - \exp(-k_{obs}t)) \quad (5)$$

where *F* is the fluorescence at time *t*, y_0 is the fluorescence intensity at $t = 0$, *a* and k_{obs} are the amplitude and the observed rate constant, respectively. To calculate the K_d as a ratio of the rate constants, the observed rate constants were plotted vs concentration of the protein and the linear fit (as for the simple bimolecular reaction) gave the association rate constant, k_{on} (a slope of the line), and a dissociation rate constant, k_{-off} (*y*-intercept of the line). The theoretical dissociation rate constant calculated from the graph was compared to one observed experimentally using heparin trap solution (*34*).

RESULTS AND DISCUSSION

Purification and Activity of XPA and RPA. Recombinant xXPA and hRPA were purified as described in Materials and Methods and shown in Figure 1. N-terminal amino acid sequencing and electrospray ionization mass spectrometry confirmed the predicted sequence, molecular weight, and homogeneity of the prepared samples (*22*). Size-exclusion chromatography demonstrated that the highly purified proteins existed as single species in solution (*23*). Activity of recombinant xXPA was confirmed using efficient DNA repair extracts derived from *Xenopus* oocytes, i.e., an antibody specific for XPA inactivated repair, which was then restored by addition of the recombinant xXPA (*32*). Neither recombinant protein contained affinity tags (e.g., His-Tag) that might be involved in fluorescein protonation and significantly influence binding parameters. Both xXPA (Figure 1B) and RPA (not shown) also exhibited DNA binding by gel mobility shift assays and both proteins bound DNA with nM binding constants (see below).

Fluorescein Is a NER Lesion. Exploiting the sensitivity of fluorescence methods requires the presence of a fluorescent signal on at least one of the reactants. If none of the molecules exhibit sufficient intrinsic fluorescence, it is necessary to add a fluorescent label to the system, ideally without significantly perturbing the relevant interactions. Fluorescein is a widely used fluorescent label that resembles a bulky DNA lesion, so it may provide both a sensitive indicator of protein binding to DNA as well as a relevant NER substrate. The *E. coli* UvrABC system acts upon

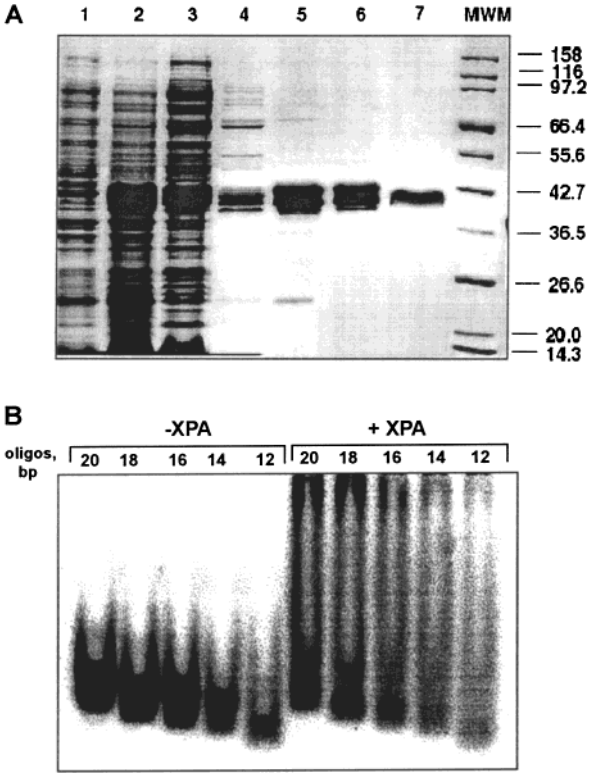

FIGURE 1: Purification of recombinant *Xenopus laevis* XPA protein and confirmation of its activity by EMSA. (A) 10% SDS−PAGE of xXPA purification with Coomassie staining. xXPA was expressed and purified as described in Materials and Methods. Lane 1, uninduced whole-cell lysate; 2, induced bacterial cell lysate; 3, soluble fraction prior to purification; 4, pooled HQ-chromatography fractions; 5, pooled HS chromatography fractions; 6, pooled HIC chromatography fractions; 7, HIC-fractions following ioadoacetamide treatment (*23*); MWM, broad range protein markers, New England BioLabs (Beverly, MA). Mobility of intact xXPA corresponds to ~40 kDa despite a calculated MW of 30.9 kDa (*23*). (B) xXPA exhibits gel mobility shifts with undamaged 12−20 bp ds oligonucleotides. Electrophoresis time was limited to prevent the 12 bp oligonucleotide from running off the gel. Experiments using longer electrophoresis times (not shown) demonstrate that the complex entered the gel, consistent with formation of soluble XPA−DNA complexes rather than aggregates.

fluorescein as efficiently as known lesions (R. Walker, unpublished data). We prepared a covalently closed circular ds DNA containing a single defined fluorescein as described in Materials and Methods and shown in Figure 2A. This substrate was readily repaired in our *Xenopus* nuclear extracts by NER (Figure 2B), and the resulting ^{32}P-labeled plasmid no longer contained fluorescein when analyzed on a Molecular Dynamics FluorImager. Repair was obliterated by XPA antibody, demonstrating a requirement for XPA. As expected with our high signal-to noise repair extracts (*31*), only plasmids containing a single fluorescein (duplicate lanes 3 and 4) incorporated radioactivity, while lesion-free control plasmid did not. Thus, DNA containing fluorescein is a substrate for NER.

Competition experiments between fluorescein-labeled oligonucleotide ds50 and either UV-irradiated oligonucleotides or plasmids containing known bulky adducts (cyclobutane pyrimidine dimers and pyrimidine (6−4) pyrimidone photodimers) are consistent with the finding that fluorescein is a lesion (Figure 2C). Qualitatively, the oligonucleotides are ~5−10 times better competitors than the plasmid, and UV-

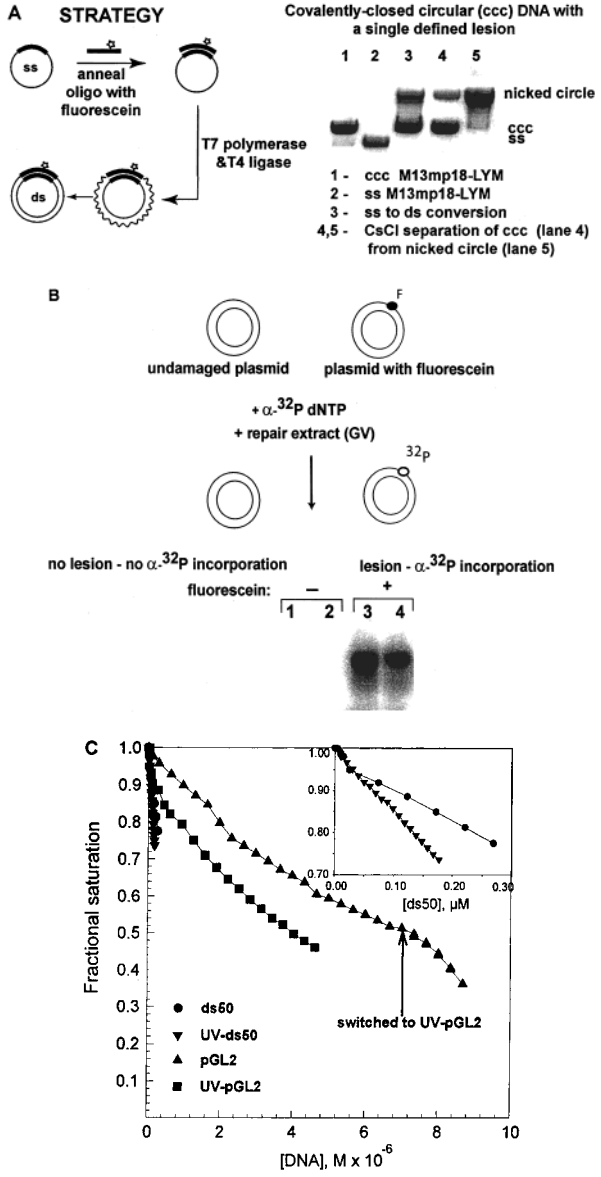

FIGURE 2: Fluorescein is recognized as a lesion and repaired by *Xenopus* oocyte nuclear extracts. (A) Preparation of substrate containing a single defined lesion. ss oligonucleotide containing a single fluorescein was annealed to ssM13mp18 and a complementary-strand synthesis was performed as described in Materials and Methods. The right panel shows separation on a 1% agarose gel of nicked circular from covalently closed circular DNA and ss template. We have successfully produced 5 mg of covalently closed circular plasmid containing a single defined lesion. (B) A single defined fluorescein in a plasmid is repaired by *Xenopus* nuclear extracts. Conditions were as described in Materials and Methods. Only those plasmids containing a single fluorescein (duplicate lanes 3 and 4) incorporated radioactivity, while lesion-free control plasmid did not. (C) Competition between fluorescently labeled oligonucleotide and DNA ± UV irradiation. Fluorescence intensity measurements were performed by mixing 10 nM of fluorescently labeled ds50 and 100 nM xXPA in 10 mM potassium phosphate, pH 7.5, 100 mM KOAc, 1 mM EDTA, 10% glycerol, and then challenging with increasing concentrations of the indicated unlabeled competitors. The competitors were added in microliter aliquots and allowed to equilibrate for 3−5 min before measurement. The competitors consisted of ds50 (●), UV-ds50 (▼), pGl2 (6046 bp) (▲), and UV-pGL2 (■). UV irradiation at 254 nm (400 mJ/cm^2) corresponds to approximately one cyclobutane pyrimidine dimer per 50 bp. The ordinate values are expressed as $[1 - (F - F_{min})/(F_{max} - F_{min})]$; the abscissa indicates increasing concentration of the competitors. Inset displays an expanded ordinate for UV-ds50 and unlabeled ds50.

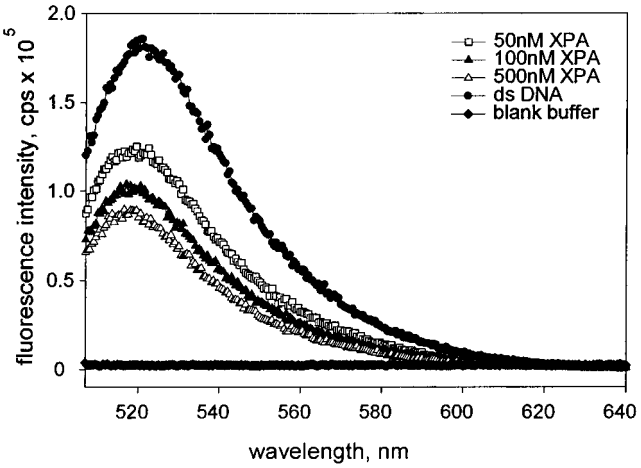

FIGURE 3: Steady-state fluorescence emission spectra of 5′-labeled oligonucleotide is quenched upon xXPA addition. The fluorescence emission spectra of ds50 oligonucleotide in buffer D were recorded in the presence of increasing amounts of xXPA (50, 100, and 500 nM) at 25 °C. The DNA concentration was 10 nM. Protein fluorescence was at background level (not shown). The spectra were recorded by scanning between 507 and 640 nm with 495 nm excitation wavelength.

irradiated competitor is ∼2−4-fold better than nondamaged. A major difference between the ds50 ± UV and plasmid is the concentration of ends. If end-binding is significant, then any ds50 competition experiments will underestimate increased binding to damage by XPA. This finding may partially explain the wide variations in reported K_d values and relatively low specificity for damage with XPA, i.e. damage recognition might be obscured by end-binding. Although future experiments with well-defined substrates will test this hypothesis, the observed changes in fluorescence intensity (Figure 2C) demonstrated the feasibility of quantitative binding measurements between XPA and fluorescein-labeled DNA.

Fluorescence changes occurring upon binding of xXPA to the 7-kb plasmid containing a single fluorescein (Figure 2C) were too weak for accurate estimation of K_d. This might be due to limited accessibility of fluorescein to xXPA either because of the intrinsic structure of supercoiled plasmid vs linear oligonucleotides or fluorescein intercalation and subsequent quenching. Indeed, the fluorescence signal from plasmid was significantly lower than that from 5′-end labeled oligonucleotide. If the fluorescence signal with supercoiled substrate can be enhanced, then future experiments evaluating torsional effects on recognition/binding can be addressed. Initial binding experiments with an oligonucleotide containing an internal fluorescein produced some fluorescence intensity changes, although they were insufficient for calculating a reliable K_d. However, the change in the amplitude of the fluorescence signal was significantly better for the 5′-end labeled oligonucleotide that was used in our subsequent binding measurements.

Fluorescence Quenching. The steady-state fluorescence emission spectra of the 10 nM fluorescently labeled oligonucleotide ds50 (filled circles) in binding buffer D, and significant fluorescence quenching, upon xXPA binding is shown in Figure 3. Fluorescence quenching is dependent on xXPA concentration and reaches saturation at 500 nM xXPA. Further increase of xXPA concentration did not change the fluorescence intensity. The emission spectra were recorded

by scanning from 507 to 640 nm with 495 nm excitation wavelength. The emission maximum of labeled ds50 is 520 nm, and it did not shift upon binding to the protein. Both the binding buffer and xXPA protein have a negligible fluorescence at indicated wavelengths. Similar fluorescence quenching occurs with ss50 and RPA in binding buffer E (not shown).

Overview of Fluorescence Binding Measurements. Here we applied fluorescence equilibrium and kinetic approaches to protein−DNA interactions with the goal to uncover steps involved in the process of damage recognition in DNA repair. Our experiments were designed to test whether xXPA ± RPA binding to fluorescein-labeled oligonucleotides is relevant to formation of damage-recognition protein complex during DNA repair. True equilibrium and kinetic analyses methods can reveal whether binding reactions are consistent with multistep processes, involving binary, tertiary, etc., complexes, and provide estimates for binding affinities in solution. To study the interaction of these proteins with oligonucleotides, we used fluorescence equilibrium (intensity and anisotropy) and stopped-flow kinetic measurements. Fluorescence of labeled oligonucleotides is quenched ~50% upon titration with xXPA (Figure 4) or RPA (Figure 5). The dissociation constant K_d measured by equilibrium was calculated as described in Materials and Methods.

Fluorescence anisotropy is sensitive solely to the size of the binding components assuming identical buffers, temperature, viscosity, etc., and it provides another estimate of the K_d. The binding of xXPA to the labeled oligonucleotide increases anisotropy from 0.07 for free oligonucleotide to 0.17 for the protein−DNA complex (Table 1), in agreement with an XPA/RPA study utilizing oligonucleotides containing 3′-end fluorescein (*17*). Interestingly, this analysis reported the affinity of RPA for 3′-fluorescein-labeled oligonucleotide was 30% higher vs. unmodified DNA. Moreover, the fluorescence intensity changes upon binding were not observed. Our data showed up to 87% fluorescence intensity quenching when xXPA or RPA interact with our 5′-labeled DNA. Interpretation of anisotropy results can be extremely complicated when significant fluorescence intensity changes occur upon binding. We found the intensity changes measured in our equilibrium and kinetic studies using the broad range of DNA concentrations to be more sensitive and reliable for direct measurements of the binding parameters in comparison to anisotropy changes.

Stopped-flow kinetic methods investigate the mechanism of protein−DNA interactions in real time and reveal the association (k_{on}) and dissociation (k_{off}) rate constants. The k_{off}/k_{on} ratio also provides an additional estimate for the dissociation constant K_d for comparison to the K_d values derived from equilibrium methods. The nanomolar K_d values determined by both equilibrium and stopped flow methods agree well (Table 2), demonstrating that the system used in this study exhibits behavior amenable to characterized spectrofluorometric methodologies.

XPA Equilibrium Binding Measurements. Figure 4 presents the equilibrium binding measurements of ds50 (5, 20, and 50 nM) and ss50 (10 nM) titrated with increasing amounts of xXPA. Fluorescence of DNA is quenched upon interaction with xXPA. Global analyses of all three ds binding isotherms in terms of single internally consistent K_d was performed, and a K_d of 24.4 ± 2.5 nM was calculated. This indicates

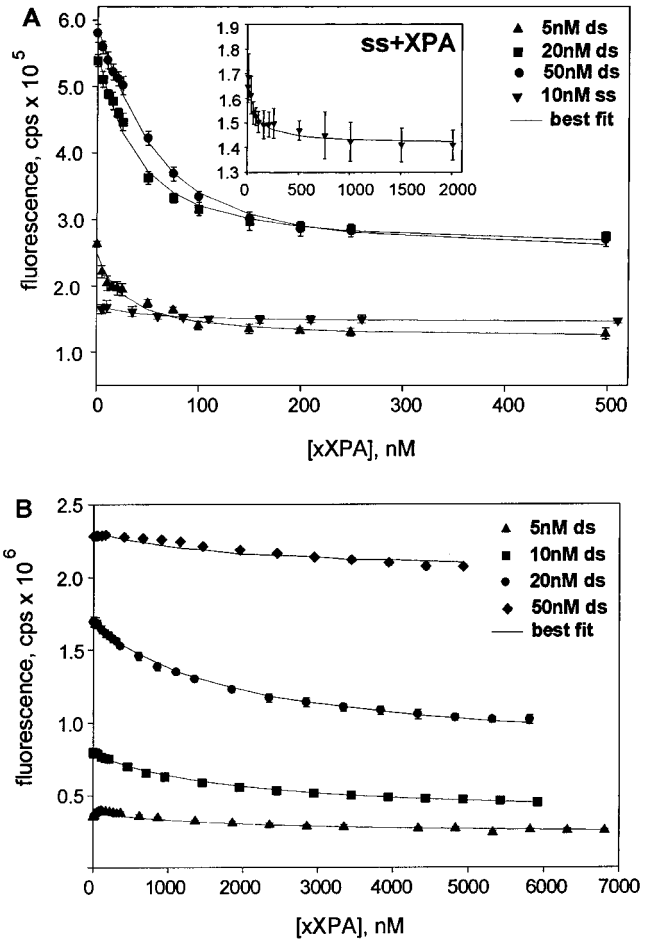

FIGURE 4: Equilibrium binding measurements of xXPA with ds and ss oligonucleotides. (A) The titrations in buffer D were performed at the indicated ds50 and ss50 concentrations of 5, 20, and 50 nM and increasing xXPA. The data were fit using nonlinear least-squares regression analysis. Global analysis of the data yielded a single K_d of 24.4 ± 2.5 nM for ds50. Inset displays an expanded ordinate for ss50 data. (B) Measurements of xXPA binding to ds50 in buffer E were performed at the indicated concentrations. The calculated K_d is 1.970 ± 0.226 μM.

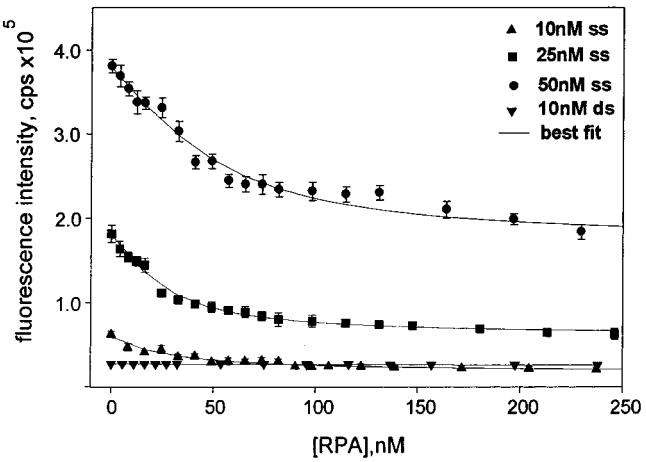

FIGURE 5: Equilibrium binding measurements of RPA with ss and ds oligonucleotides. Equilibrium binding measurements in buffer E at the indicated ss50 concentrations yielded K_d = 20.3 ± 2.5 nM. The binding of RPA to ds50 is very weak (>1 mM).

strong affinity between xXPA and ds DNA in buffer D that is 5−1000 times higher than reported for gel shift, filter binding, or surface plasmon resonance experiments with

Table 1: Fluorescence Anisotropy Measurements of xXPA and RPA to DNA Substrates[a]

DNA	protein	anisotropy free	anisotropy bound	Δ anisotr. units	Δ anisotr. %	Δ intensity %
ds 50	xXPA	0.066	0.169	0.103	256	−87
	RPA	0.065	0.08	0.015	123	−6
ss 50	xXPA	0.036	0.078	0.042	217	−15
	RPA	0.025	0.22	0.195	880	−86

[a] Binding buffer D was used for xXPA binding measurements, and buffer E was used for RPA binding measurements. Fluorescence anisotropy was calculated according to eq 2.

0.05−3.5 kb substrates containing zero to multiple UV-lesions and performed using different binding buffers.

Interestingly, equilibrium measurements using the same DNA and protein but in buffer E yielded a strikingly different K_d of 1.970 ± 0.226 μM (Figure 4B). The ~80-fold K_d difference cannot be explained as an artifact such as general protein/DNA precipitation because buffer E was used to yield a nanomolar K_d for the same DNA and RPA (Figure 5). This result might be explained by different ionic strengths of the buffers; buffer D (Tris-OAc) is 0.151 M and buffer E (HEPES) is 0.257 M. While future experiments in buffer systems of equal ionic strength could be tested to identify particular components responsible for K_d differences, our results demonstrate the xXPA−DNA binding reaction is extremely sensitive to solution conditions, and this observation may partially explain some of the reported fluctuations in K_d values measured by EMSA, SPR, and filter binding assays.

Unlike our xXPA, all other reported binding measurements were performed using human XPA that contained an N-terminal His-Tag. For example, His-Tag-XPA binding to a ds 49 bp oligonucleotide in 30 mM HEPES, pH 7.8, 100 mM NaCl, 5 mM $MgCl_2$, 0.5% inositol, 1 mM DTT (ionic strength 0.07 M), revealed $K_a = 1.2 \times 10^7$ M^{-1} (corresponding to K_d = 83.3 nM) using EMSA (*19*). A recent fluorescence anisotropy report using His-Tag-XPA and 36-mer oligonucleotides containing fluorescein at the 3′-end found binding was also strongly salt-dependent (*17*). The K_d for ds DNA (1150 nM) determined in this study with XPA binding buffer (20 mM Tris-Cl, pH 7.5, 50 mM NaCl, 2 mM $MgCl_2$, 1 mM DTT, 100 ng/μL BSA, 10 μM $Zn(OAc)_2$, 0.1 mM polyoxydecyl ether, 10% (v/v) glycerol, ionic strength 0.072 M), was nearly 50-fold higher than we report for buffer D (ionic strength 0.15 M), but similar to our K_d measured in buffer E (ionic strength 0.225 M).

The K_d for ss DNA consisting of a mixed purine−pyrimidine sequence in the same study was 355 nM; however, it was 170 nM for a pyrimidine-rich sequence, and greater than 3 μM for a purine-rich sequence. The K_d reported for ss DNA by surface plasmon resonance (SPR) was 13 nM (*16*) and by EMSA was 217 nM (calculated from the reported K_a (*19*)). Analysis of our data (Figure 4A) yielded a K_d in the nanomolar range based on the minimal fluorescence intensity changes for ss as compared to ds DNA. It is difficult to obtain a reliable K_d for ss DNA binding from these data for comparison to the markedly divergent earlier reports. The error bars for the ss50 fluorescence measurements are large, and the fluorescence changes that occur upon xXPA binding are minimal as compared to ds 50.

There are many possibilities to explain the K_d differences among the above-noted independent studies. Plausible factors include different locations of the fluorescein (5′- vs 3′-ends), the presence and absence of the His-Tag in XPA protein, DNA sequence variations and/or oligonucleotide lengths, and different ionic strength of binding buffers. In our study, the best data fits and lowest K_d values correlated with the maximal fluorescence intensity changes. Thus, selection of our binding buffers was determined empirically to avoid high error estimates of K_d values. The same buffers could not be used for both XPA and RPA measurements due to the minimal fluorescence changes that occurred upon RPA binding to ss DNA in Tris-OAc. In future studies, it would be interesting to investigate if efficient NER could occur in the buffer systems used for our binding studies and then relate these results to events during NER in vivo.

RPA Equilibrium Binding Measurements. Equilibrium binding measurements in buffer E at increasing RPA concentrations with 10, 25, and 50 nM ss50 yielded K_d of 20.3 ± 2.5 nM (Figure 5). No significant fluorescence intensity changes were observed in our system upon RPA binding to ds50 DNA in agreement with the weak binding to a ds 49-mer reported by EMSA (*18*, *19*), but in contrast with an anisotropy study that reported K_d of 245 ± 36 nM (*17*). Earlier studies on RPA interaction with different substrates demonstrated that binding affinity of RPA for short oligonucleotides was length dependent, and its apparent association constant for 10-mer oligonucleotides and 50-mer varied over 200-fold (*28*). Moreover, the stoichiometry of RPA binding for different length olinucleotides varied as well. For example, interaction with poly-dT20 and poly-dT30 revealed a 1:1 stoichiometry of RPA binding, while poly-dT70's stoichiometry was 3 (*28*). Poly-dT50 would be most relevant to our ss50 oligonucleotide, but stoichiometry for either poly-dT50 or poly-dT60 were not determined in this study. Two binding modes have been identified for RPA: an initial binding to a minimal 8−10 nucleotide region (*37*) followed by an approximately 100-fold more stable 30-nucleotide binding mode (*28*, *38*). Using oligonucleotides containing hairpin structures with 3′- or 5′-protruding ss arms, initial DNA binding occurs at the 5′-oriented site of RPA with a proposed transition to the ~30-nucleotide mode requiring stretching of RPA along the DNA in a 3′-direction (*39*). Overall, RPA binds DNA with low cooperativity, and the binding sites on DNA are not equivalent; in fact, RPA may have a preference for binding to the ends of DNA (*28*).

Earlier in this study, we showed that xXPA was extremely sensitive to binding buffer, i.e., the K_d values for ds50 differed by 3 orders of magnitude between buffer D and the buffer used to measure RPA interaction with ss50 (buffer E). Similarly, RPA was sensitive to binding buffer, and no fluorescence intensity changes were observed when buffer D was substituted for buffer E. Interestingly, no binding could be detected by spectrofluorometry when buffer F, used to determine RPA binding constants by gel mobility shift assays (*28*), was tested in our study. Thus, both XPA and RPA are very sensitive to solution conditions.

The issue of RPA as a damage recognition protein is somewhat controversial. NER requires RPA-dependent opening around the lesion, with RPA probably binding the undamaged strand (*39*). Like XPA, RPA is known to interact with multiple repair proteins; besides XPA (*40*, *41*), these

Table 2: Summary of the Stop-Flow and Equilibrium K_d for xXPA and RPA Binding to Various DNA Substrates[a]

DNA + protein	K_{on} ($\times$ 10(8) M^{-1} s^{-1})	K_{off} (s^{-1})	K_d stop-flow (nM)	K_d equilibrium (nM)
ds 50 + XPA	9.03 ± 0.045	26.1 ± 0.13	28.9 ± 0.14	24.4 ± 2.5
ss 50 + RPA	0.598 ± 0.003	5.74 ± 0.03	96.0 ± 0.48	20.3 ± 2.5
ds50-4M + XPA	2.41 ± 0.063	38.1 ± 0.99	158 ± 4.1	ND
ds50-4M + [XPA + RPA]	0.193 ± 0.008	47.36 ± 1.89	245.4 ± 9.8	ND

[a] xXPA and xXPA-RPA binding measurements were performed in binding buffer D, while RPA measurements used binding buffer E. ND = not determined. All data fits were done assuming 1:1 stoichiometry. Poor data fits occurred at other stoichiometries (not shown).

include XPG and ERCC1-XPF (*39*, *40*, *42*, *43*). RPA was proposed as a damage recognition factor because it has some affinity for damaged DNA (*41*, *44*, *45*). The recent finding that it binds to the undamaged strand (*39*) supports its role in facilitating damage recognition. RPA alone or together with XPA and/or other factors may sense single-stranded propensity resulting from lesion-induced helical distortion. Furthermore, Wold and co-workers (*19*) recent findings with DNA containing a (6−4) lesion suggest that RPA probably binds to both damaged and undamaged strands during NER, although fluorescence anisotropy reported the presence of cisplatin modification weakens binding of RPA to ss DNA (*17*). Thus, the effects of DNA lesions on RPA binding remain unresolved.

Anisotropy Measurements. Steady-state fluorescence anisotropy is a powerful method for the study of molecular interactions, provided the data is corrected for intensity changes and acquired at multiple substrate concentrations (*46*). Small molecules rotate quickly during the excited state, and upon emission, have low anisotropy values. Large molecules, or molecules that become larger as a consequence of binding a second molecule, rotate little during the excited state, and therefore have high anisotropy values. Thus, the change in anisotropy value is the direct indication of molecular interactions. Binding of the protein to an oligonucleotide causes an increase in the rotational correlation time and, consequently in the anisotropy value due to the increased size of the oligonucleotide-protein complex as compared to the free oligonucleotide (*47*). The increase in anisotropy can also be due to reduced angular motion of the fluorescent probe's close contact with an interacting protein. The complexity of interactions in our system together with significant change in fluorescence intensity prohibits definitive resolution of the contributions from various forces toward binding. Therefore, our anisotropy data analysis was for qualitative comparisons of protein(s) binding to DNA rather than for quantitative determination of dissociation constants.

Table 1 shows the anisotropy change of ds and ss oligonucleotides upon binding to xXPA and RPA. As expected, anisotropy of ss50 is ~2 times lower than ds50, and it increases after titration with proteins. The greatest increment in anisotropy value is observed upon ss50-RPA complex formation (Table 1). Considering the polarity of RPA binding to ss DNA (*39*) and the presence of fluorescein label on the 5′-end of the oligonucleotide, this result can be explained by both a decrease in global tumbling of the complex and restriction of fluorescein's local motion upon its direct interaction with RPA. The smallest anisotropy change was observed for RPA binding to ds50 (Δ 0.015 units) and xXPA binding to ss50 (Δ 0.042 units), which is consistent with smaller intensity changes (6 and 15% decrease, respectively) suggesting weaker binding. This result agrees with our data collected by the equilibrium titration approach (Figures 4A and 5). Thus, fluorescence anisotropy can provide a reliable solution-based methodology for monitoring protein binding to DNA if performed at multiple concentrations of the binding components and properly corrected by fluorescence intensity changes.

Stop-Flow XPA Binding Measurements. To further understand the mechanism of XPA and RPA interaction with ss and ds DNAs in real time and to compare the binding constants derived from equilibrium data, the fast kinetics of these interactions were investigated for the first time using stopped-flow methods.

Decrease in DNA fluorescence upon complex formation was measured by rapidly mixing xXPA and fluorescently labeled ds or ss oligonucleotide from two separate syringes in buffer D. Representative stopped-flow traces for three increasing xXPA concentrations (25, 50, and 100 nM) and constant ds50 concentration (10 nM) are presented in Figure 6A. Kinetic traces for seven increasing concentrations of xXPA (10 to 200 nM) were fit to the single exponential eq 4 and the observed rate constants were plotted vs xXPA concentration to obtain association k_{on} (slope of the linear fit) and dissociation k_{off} (y-intercept of the linear fit) rate constants (Figure 6B). The linear increase of the observed rate constant with increasing xXPA concentration indicates that complex formation can be described by an apparent bimolecular reaction. The formation of xXPA−DNA complex occurs at a relatively fast rate with $k_{on} = 9.03 \times 10^8$ M^{-1} s^{-1}, and the dissociation of the resulting complex is also rather fast with $k_{off} = 26.1$ s^{-1}. The ratio k_{off}/k_{on} yielded $K_d = 28.9$ nM. Thus, our K_d determined from equilibrium studies ($K_d = 24.4$ nM) is in excellent agreement with stop-flow kinetic derived K_d (Table 2). This consistency in the K_d values by two independent methods demonstrates the measured on and off rates are an adequate description of the xXPA-ds50 interaction process.

Interestingly, on and off rates for XPA−DNA interactions using His-Tag-XPA and a lesion-free ds 70-mer determined by SPR ($k_{on} = 5.0 \times 10^4$ M^{-1} s^{-1}, $k_{off} = 2.62 \times 10^{-3}$ s^{-1}) (*16*) were significantly different from those reported here, although the K_d value was just 2 times higher (57.8 vs 28.9 nM, respectively). All XPA binding measurements by SPR required increased ligand concentrations and densely derivatized DNA surfaces (2000 RU) to detect *any* XPA−DNA binding. Thus, the discrepancy in measured kinetic parameters between SPR and our solution-based equilibrium and stop-flow studies might be explained by multiple factors, including the sensitivity to different binding buffers (Figure 4A,B), biotinylated DNA probes, or the addition of 22 N-terminal amino acids containing a His-Tag to XPA protein.

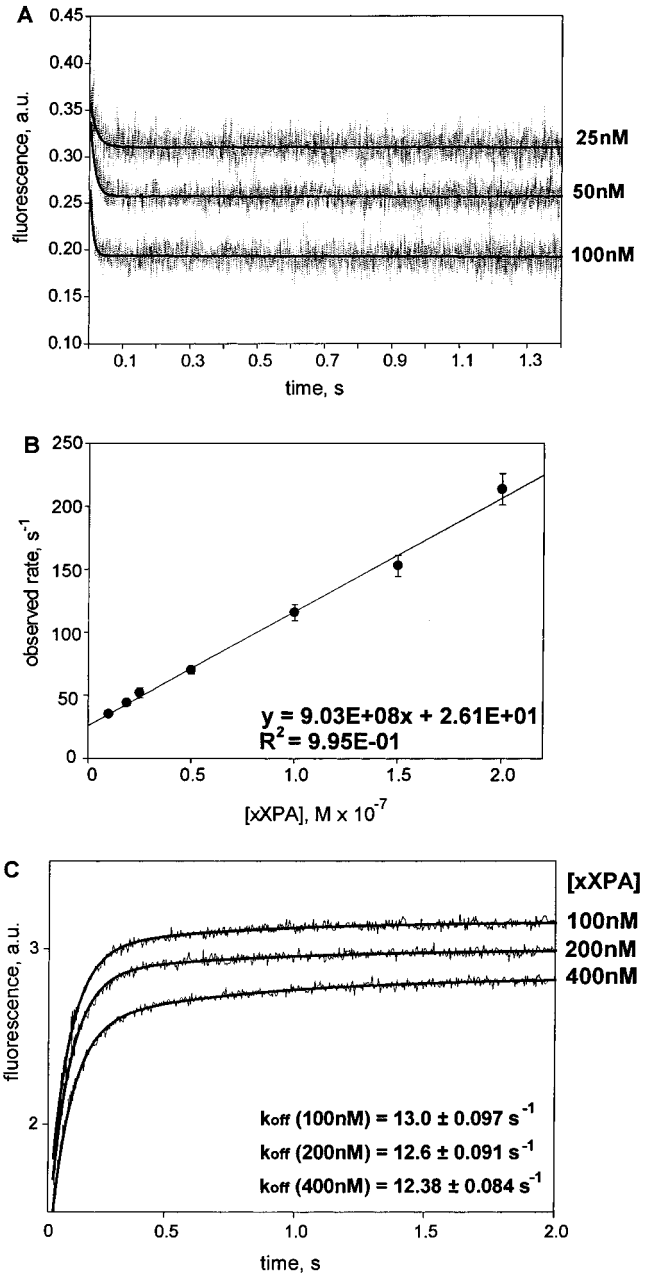

FIGURE 6: Stop-flow kinetic binding measurements of xXPA to ds50 oligonucleotide. (A) Representative kinetic data shows the time-dependent decrease in ds50 fluorescence after mixing 10 nM ds50 with 25, 50, and 100 nM xXPA. The kinetic trace is an average of 11 measurements. The solid line is the best single-exponential fit to the data. (B) The observed rate constants from panel A were plotted vs [xXPA] and the resulting linear fit yielded $k_{on} = 9.03 \pm 0.045 \times 10^8$ M^{-1} s^{-1} (slope) k_{off} (intercept) of 26.1 $\pm$ 0.13 s^{-1}. The ratio k_{off}/k_{on} provided K_d of 28.9 $\pm$ 0.14 nM. (C) Heparin-trap experiment to measure off-rate at varying xXPA concentrations. Preformed xXPA−DNA complexes in buffer D at the indicated [xXPA] and 10 nM ds50 were disrupted by rapid mixing with a heparin trap solution. Increasing fluorescence demonstrates xXPA was not aggregating and k_{off} values of 13.0 $\pm$ 0.097, 12.6 $\pm$ 0.091, and 12.38 $\pm$ 0.084 s^{-1} at 100, 200, and 400 nM xXPA, respectively, were derived from the kinetic traces.

No time-dependent fluorescence changes were observed when ss50 was mixed with xXPA in binding buffer D, consistent with equilibrium data exhibiting minimal intensity changes when xXPA interacts with ss50 (Figure 4A). Similar results were observed when buffers E or F were used.

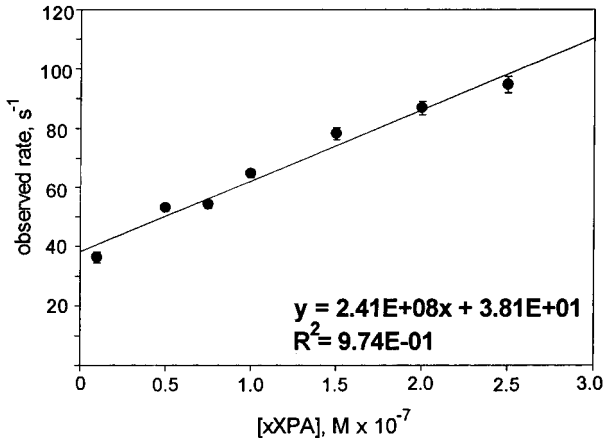

FIGURE 7: Stop-flow kinetics measurements for XPA binding ds50 oligonucleotide with a 4-bp mismatch. The observed rate constants were plotted vs [xXPA] and the resulting linear fit yielded k_{on} of $2.41 \pm 0.063 \times 10^8$ M^{-1} s^{-1} and k_{off} of 38.1 $\pm$ 0.99 s^{-1}. The ratio k_{off}/k_{on} provided K_d of 158 $\pm$ 4.1 nM. ds50 concentration was 10 nM.

The dissociation rate constant for xXPA and ds50 was determined here using two approaches: as a *y*-intercept of the linear fit of the observed rate (Figure 6B) and experimentally, using a heparin trap solution (Figure 6C). Preformed xXPA−DNA complexes in buffer D at various xXPA concentrations and 10 nM ds50 were disrupted by rapid mixing with a heparin trap solution from a separate syringe. The increasing fluorescence of ds50 demonstrates that the complexes dissociate under these conditions and also shows there is no significant aggregation of xXPA and/or DNA in the binding experiments. The kinetic traces were fit to the single exponential eq 5 and yielded dissociation rate constants k_{off} of 13.0, 12.6, and 12.4 s^{-1} at 100, 200, and 400 nM xXPA, respectively (Figure 6C). Thus, heparin addition to XPA−DNA complexes yielded a single exponential off-rate, and the fluorescence intensity of the DNA returned to its original value, while heparin added to control DNA did not cause an intensity change. These observations are consistent with a competition effect. Heparin was reported to disrupt other protein−DNA binding interactions, e.g., refs *48*−*51*. The relatively close agreement between the k_{off} determined experimentally (12.7 s^{-1} average) using heparin trap solution and k_{off} calculated from the *y*-intercept of the observed rate fit (26.1 s^{-1}) again provide an independent consistency for our experiments. Furthermore, identical results were obtained on two different spectrofluorometers, an Aviv ATF105 and a Molecular Kinetics SFM-4/Q, averaged over 10 experiments each.

A recent DNA damage-recognition model proposed that loss of hydrogen bonding contacts between bases on complementary DNA strands is an essential signal to recruit NER proteins (*18*). To test this hypothesis, we applied stop-flow kinetics measurements for xXPA binding to fluorescently labeled ds50 containing mispaired bases located in the central region of the oligonucleotide (Figure 7). The linear fit of the data shows that xXPA binds to this DNA with a 4-fold slower k_{on} than to the homoduplex substrate (2.41×10^8 vs 9.03×10^8 M^{-1} s^{-1}) and dissociates faster with a k_{off} = 38.1 s^{-1} (vs 26.1 s^{-1}). The ratio k_{off}/k_{on} yielded a 5-fold higher K_d (158 $\pm$ 4.1 nM), thereby demonstrating weaker binding of xXPA to mismatched DNA. Comparison of xXPA's K_d values for homoduplex ds50 and mispaired ds50

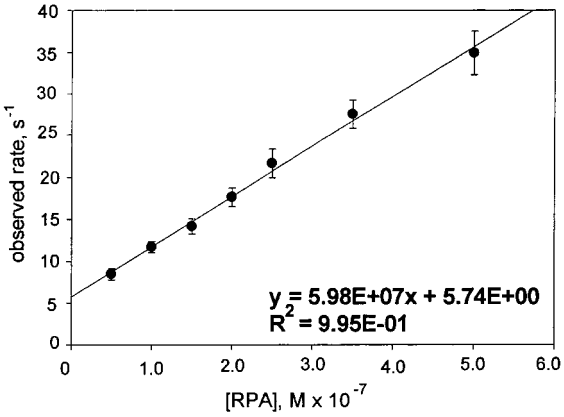

FIGURE 8: Stop-flow kinetics measurements for RPA binding ss50 oligonucleotide. The linear fit of the observed rate constants yielded k_{on} of 0.598 ± 0.003 × 10^8 M^{-1} s^{-1} and k_{off} of 5.74 ± 0.03 s^{-1}. The ratio k_{off}/k_{on} provided K_d of 96.0 ± 0.48 nM.

(28.9 vs 158 nM) shows that the difference in K_d values is mainly determined by the difference in k_{on} but not k_{off} rates for these two substrates (Table 2). Our ~7 times higher K_d for ds50−4M vs ds50 was opposite to the K_d trend reported by an anisotropy study that used a 36-mer containing six mismatches, i.e., 380 ± 45 nM for the mismatch substrate vs 1150 ± 84 for the complementary DNA (*17*).

EMSA experiments under conditions of limited protein with a 19-mer containing three mispaired bases immediately adjacent to a nondistorting pivaloyl moiety on the C4′ of a deoxyribose residue showed preferential XPA binding as compared to homoduplex oligonucleotide, and no binding to ss DNA (*18*). Our results are not directly comparable with this study due to the substrate differences, i.e., length, lesion type, and distance from mispaired bases. A potential model to explain our data is that too much helical distortion, such as 4 bp, begins to resemble the post-damage recognition step in NER, where strong XPA binding is no longer required. Once a sufficiently large single-stranded region forms as a consequence of recruiting other repair proteins, XPA binds DNA less tightly and dissociates. Future spectrofluorometric experiments with a series of well-defined substrates containing mismatches of varying lengths at various locations relative to the lesion may resolve this issue.

Stop-Flow RPA Binding Measurements. Equilibrium binding demonstrated the expected high affinity of RPA to ss50 oligonucleotide. To determine the kinetic parameters of this interaction using fluorescence spectroscopy, the binding of RPA to DNA was studied by stop-flow methods. The conditions were the same as for the equilibrium measurements. Seven increasing concentrations of RPA (50−500 nM) and constant ss50 concentration (10 nM) produced kinetic traces that were fit to a single exponential (eq 4) to obtain observed rates (Figure 8). Linear fit of the observed rates yielded very slow $k_{on} = 0.598 \times 10^8$ M^{-1} s^{-1} and $k_{off} = 5.74$ s^{-1} that are indicators of kinetically stable binary complex. These rates translate into $K_d = 96$ nM. Although the k_{on} determined by SPR (*16*) is comparable to our k_{on} (1.21 × 10^7 vs. 5.98 × 10^7 M^{-1} s^{-1}), there are 4 orders of magnitude difference between the k_{off} values, resulting in very different K_d values. One possible explanation for this discrepancy is that the immobilized DNA substrates in SPR may affect the k_{off}.

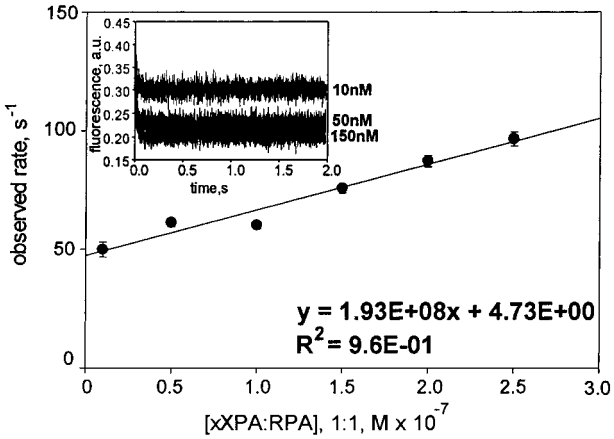

FIGURE 9: Stop-flow kinetics measurements for xXPA−RPA complex binding to ds50−4M oligonucleotide with 4-bp mismatch. The observed rate constants were plotted vs [xXPA-RPA], and the resulting linear fit yielded k_{on} of 0.193 ± 0.008 × 10^8 M^{-1} s^{-1} and the k_{off} of 47.36 ± 1.89 s^{-1}. The ratio k_{off}/k_{on} provided K_d of 245.4 ± 9.8 nM. ds50−4M concentration was 10 nM. Inset shows three representative kinetic traces of this binding. Each trace is an average of 11 measurements.

The equilibrium K_d value obtained from our fluorimetric titrations is, however, lower than K_d derived from the kinetic rate constants (Table 2). The difference in K_d values from these two methods suggests the presence of an additional step in the binding. This step may be very fast (beyond fluorometer's resolution) or very slow, and it was not observed by our stopped-flow kinetic measurements. Considering the fact that RPA binds DNA with low cooperativity, the possibility exists that one of the approaches was unable to detect the cooperativity factor, which might significantly contribute to K_d.

Stop-Flow XPA + RPA Binding Measurements. We showed that xXPA binds ds50 containing 4 bp mismatch with ~6-fold lower affinity than completely complementary ds50. Because XPA is known to form a tight stoichiometric complex with RPA (*52*), we decided to determine the binding constant of this protein complex to the ds50 mispaired substrate by stop-flow kinetic analysis. xXPA and RPA were mixed at equimolar amounts and reacted with ds50−4M (Figure 9). The on-rate of the complex was somewhat similar to RPA and ss50 on-rate, and the off-rate was comparable to xXPA and ds50−4M interaction (Table 2). The K_d for the complex was ~1.5-fold weaker than for xXPA alone and the same substrate (245.4 vs. 158 nM). Our data suggests that both xXPA and xXPA−RPA complex have poor affinity to mispaired DNA, whereas individual proteins exhibit tight binding with nanomolar K_d to their corresponding substrates (xXPA to ds DNA and RPA to ss DNA). Assuming RPA binds ss50 analogously to the ds50M heteroduplex, the increased K_d for the xXPA−RPA complex implies the binding energies for xXPA or RPA alone are not additive. If they were, the K_d values would be femtomolar, i.e., xXPA and RPA together do not bind DNA with the same binding constants as they do separately. Thus, the increased K_d implies conformational changes or different sites of contact with DNA.

It is difficult to reconcile the rapid removal of lesions by NER with the binding data for a putative damage sensor consisting of XPA and RPA. Together RPA and XPA exhibit a lower affinity for mismatch DNA, and therefore this

complex is not a strong sensor for heteroduplexes. Our ds DNA substrate containing a 4-bp mismatch was bound 5 times weaker by xXPA, consistent with the observation that XPA prefers ds DNA. Perhaps this substrate resembles a postrecognition, unwound structure in NER in which XPA is no longer required. Future experiments with similar substrates are necessary to determine if the mismatch region represents a competitor for the fluorescein, and if it represents a primary target for binding by XPA, RPA, or XPA−RPA complex. We have already demonstrated that single-molecule fluoresecence methods can be applied to xXPA−DNA interactions with ds50 (*53*), so it is feasible to study binding events within single-molecule complexes in more detail.

ACKNOWLEDGMENT

We thank Alexander Spoonde for preliminary spectrofluorescence experiments demonstrating XPA binding to fluorescein-containing oligonucleotides and Loel Kathmann for technical assistance preparing RPA. We also thank Washington State University professors Keith Dunker and Lisa Gloss for useful discussions and access to their spectrofluorometers. We thank Greg Schenter (PNNL) for global analysis of the equilibrium data.

NOTE ADDED IN PROOF

After submission of our manuscript, Patrick & Turchi (2001, *J. Biol. Chem. 276*, 22690) reported stop-flow measurements of RPA protein with DNA ± 1,2d(GpG) cisplatin. These results are consistent with a role for RPA in DNA damage recognition.

REFERENCES

1. Lindahl, T., and Wood, R. D. (1999) *Science 286*, 1897−905.
2. Robins, P., Jones, C. J., Biggerstaff, M., Lindahl, T., and Wood, R. D. (1991) *EMBO J. 10*, 3913−21.
3. Jones, C. J., and Wood, R. D. (1993) *Biochemistry 32*, 12096−104.
4. Asahina, H., Kuraoka, I., Shirakawa, M., Morita, E. H., Miura, N., Miyamoto, I., Ohtsuka, E., Okada, Y., and Tanaka, K. (1994) *Mutat. Res. 315*, 229−37.
5. Nagai, A., Saijo, M., Kuraoka, I., Matsuda, T., Kodo, N., Nakatsu, Y., Mimaki, T., Mino, M., Biggerstaff, M., Wood, R. D., and et al. (1995) *Biochem. Biophys. Res. Commun. 211*, 960−6.
6. Kuraoka, I., Morita, E. H., Saijo, M., Matsuda, T., Morikawa, K., Shirakawa, M., and Tanaka, K. (1996) *Mutat. Res. 362*, 87−95.
7. Guzder, S. N., Sung, P., Prakash, L., and Prakash, S. (1993) *Proc. Natl. Acad. Sci. U.S.A. 90*, 5433−7.
8. Mu, D., Wakasugi, M., Hsu, D. S., and Sancar, A. (1997) *J. Biol. Chem. 272*, 28971−9.
9. Li, L., Lu, X., Peterson, C. A., and Legerski, R. J. (1995) *Mol. Cell Biol. 15*, 5396−402.
10. Stigger, E., Drissi, R., and Lee, S. H. (1998) *J. Biol. Chem. 273*, 9337−43.
11. Park, C. H., and Sancar, A. (1994) *Proc. Natl. Acad. Sci. U.S.A. 91*, 5017−21.
12. Sugasawa, K., Ng, J. M., Masutani, C., Iwai, S., van der Spek, P. J., Eker, A. P., Hanaoka, F., Bootsma, D., and Hoeijmakers, J. H. (1998) *Mol. Cell 2*, 223−32.
13. Mu, D., Hsu, D. S., and Sancar, A. (1996) *J. Biol. Chem. 271*, 8285−94.
14. Wakasugi, M., and Sancar, A. (1999) *J. Biol. Chem. 274*, 18759−68.
15. Ikegami, T., Kuraoka, I., Saijo, M., Kodo, N., Kyogoku, Y., Morikawa, K., Tanaka, K., and Shirakawa, M. (1998) *Nat. Struct. Biol. 5*, 701−6.
16. Wang, M., Mahrenholz, A., and Lee, S. H. (2000) *Biochemistry 39*, 6433−9.
17. Hey, T., Lipps, G., and Krauss, G. (2001) *Biochemistry 40*, 2901−10.
18. Buschta-Hedayat, N., Buterin, T., Hess, M. T., Missura, M., and Naegeli, H. (1999) *Proc. Natl. Acad. Sci. U.S.A. 96*, 6090−5.
19. Lao, Y., Gomes, X. V., Ren, Y., Taylor, J. S., and Wold, M. S. (2000) *Biochemistry 39*, 850−9.
20. Buchko, G. W., Ni, S., Thrall, B. D., and Kennedy, M. A. (1998) *Nucleic Acids Res. 26*, 2779−88.
21. Buchko, G. W., Daughdrill, G. W., de Lorimier, R., Rao, B. K., Isern, N. G., Lingbeck, J. M., Taylor, J. S., Wold, M. S., Gochin, M., Spicer, L. D., Lowry, D. F., and Kennedy, M. A. (1999) *Biochemistry 38*, 15116−28.
22. Iakoucheva, L. M., Kimzey, A. L., Masselon, C. D., Bruce, J. E., Garner, E. C., Brown, C. J., Dunker, A. K., Smith, R. D., and Ackerman, E. J. (2001) *Protein Sci. 10*, 560−571.
23. Iakoucheva, L. M., Kimzey, A. L., Masselon, C. D., Smith, R. D., Dunker, A. K., and Ackerman, E. J. (2001) *Protein Sci. 10*, 1353−1362.
24. Wright, P. E., and Dyson, H. J. (1999) *J. Mol. Biol. 293*, 321−31.
25. Mer, G., Bochkarev, A., Gupta, R., Bochkareva, E., Frappier, L., Ingles, C. J., Edwards, A. M., and Chazin, W. J. (2000) *Cell 103*, 449−56.
26. Czernik, P. J., Shin, D. S., and Hurlburt, B. K. (1994) *J. Biol. Chem. 269*, 27869−75.
27. Record, M. T., Jr., Lohman, M. L., and De Haseth, P. (1976) *J. Mol. Biol. 107*, 145−58.
28. Kim, C., Paulus, B. F., and Wold, M. S. (1994) *Biochemistry 33*, 14197−206.
29. Hoffman, B. J., Broadwater, J. A., Johnson, P., Harper, J., Fox, B. G., and Kenealy, W. R. (1995) *Protein Expr. Purif. 6*, 646−54.
30. Henricksen, L. A., Umbricht, C. B., and Wold, M. S. (1994) *J. Biol. Chem. 269*, 11121−32.
31. Oda, N., Saxena, J. K., Jenkins, T. M., Prasad, R., Wilson, S. H., and Ackerman, E. J. (1996) *J. Biol. Chem. 271*, 13816−20.
32. Ackerman, E. J., and Iakoucheva, L. M. (2000) *Methods: Companion Methods Enz. 22*, 188−193.
33. Kunkel, T. A., Roberts, J. D., and Zakour, R. A. (1987) *Methods Enzymol. 154*, 367−82.
34. Otto, M. R., Bloom, L. B., Goodman, M. F., and Beechem, J. M. (1998) *Biochemistry 37*, 10156−63.
35. Hamilton, W. C. (1964) *Statistics in Physical Science: Estimation, Hypothesis Testing, and Least Squares*, The Ronald Press Co., New York.
36. Bevington, P. R., and Robinson, D. K. (1992) *Data Reduction and Error Analysis in the Physical Sciences*, McGraw-Hill, New York.
37. Blackwell, L. J., and Borowiec, J. A. (1994) *Mol. Cell Biol. 14*, 3993−4001.
38. Kim, C., Snyder, R. O., and Wold, M. S. (1992) *Mol. Cell Biol. 12*, 3050−9.
39. de Laat, W. L., Appeldoorn, E., Sugasawa, K., Weterings, E., Jaspers, N. G., and Hoeijmakers, J. H. (1998) *Genes Dev. 12*, 2598−609.
40. He, Z., Henricksen, L. A., Wold, M. S., and Ingles, C. J. (1995) *Nature 374*, 566−9.
41. Saijo, M., Kuraoka, I., Masutani, C., Hanaoka, F., and Tanaka, K. (1996) *Nucleic Acids Res. 24*, 4719−24.
42. Matsunaga, T., Park, C. H., Bessho, T., Mu, D., and Sancar, A. (1996) *J. Biol. Chem. 271*, 11047−50.
43. Bessho, T., Sancar, A., Thompson, L. H., and Thelen, M. P. (1997) *J. Biol. Chem. 272*, 3833−7.
44. Clugston, C. K., McLaughlin, K., Kenny, M. K., and Brown, R. (1992) *Cancer Res. 52*, 6375−9.
45. Burns, J. L., Guzder, S. N., Sung, P., Prakash, S., and Prakash, L. (1996) *J. Biol. Chem. 271*, 11607−10.

46. Lakowicz, J. R. (1983) *Principles of Fluorescence Spectroscopy*, 1st ed., Plenum, New York.
47. LeTilly, V., and Royer, C. A. (1993) *Biochemistry 32*, 7753−8.
48. Lazarus, L. H., and Kitron, N. (1974) *Arch. Biochem. Biophys. 164*, 414−9.
49. von Hippel, P. H., Bear, D. G., Morgan, W. D., and McSwiggen, J. A. (1984) *Annu. Rev. Biochem. 53*, 389−446.
50. Straney, D. C., and Crothers, D. M. (1985) *Cell 43*, 449−59.
51. Mascotti, D. P., and Lohman, T. M. (1995) *Biochemistry 34*, 2908−15.
52. Li, L., Elledge, S. J., Peterson, C. A., Bales, E. S., and Legerski, R. J. (1994) *Proc. Natl. Acad. Sci. U.S.A. 91*, 5012−6.
53. Lu, H. P., Iakoucheva, L. M., and Ackerman, E. J. (2001) *J. Am. Chem. Soc. 123*, 9184−5.

BI011041Q